Energy Conversion and Management 74 (2013) 223–236

Contents lists available at SciVerse ScienceDirect

Energy Conversion and Management

journal homepage: www.elsevier.com/locate/enconman

Enhance heat transfer for PCM melting in triplex tube with internal–external fins

Sohif Mat [a,*], Abduljalil A. Al-Abidi [a,b,*], K. Sopian [a], M.Y. Sulaiman [a], Abdulrahman Th Mohammad [a]

[a] Solar Energy Research Institute, University Kebangsaan Malaysia, Bangi, Selangor, Malaysia
[b] Department of HVAC Engineering, Sana'a Community College, P.O. Box 5695, Sana'a, Yemen

ARTICLE INFO

Article history:
Received 20 December 2012
Accepted 5 May 2013
Available online 10 June 2013

Keywords:
Melting
PCM
Triplex tube heat exchanger
Heat transfer enhancement

ABSTRACT

Thermal energy storage is critical for eliminating the discrepancy between energy supply and demand as well as for improving the efficiency of solar energy systems. This study numerically investigates the melting process in a triplex-tube heat exchanger with phase-change material (PCM) RT82. A two-dimensional numerical model is developed using the Fluent 6.3.26 software program. Three heating methods were used to melt the PCM from the inside tube, outside tube, and both tubes. Internal, external, and internal–external fin enhancement techniques were studied to improve the heat transfer between the PCM and heat transfer fluid. Enhancement techniques were compared with the inside tube heating, outside tube heating, both tube heating as well as the finned and internally finned tube. The effects of fin length on the enhancement techniques were investigated. Using a triplex-tube heat exchanger with internal–external fins, predicted results indicated that melting time is reduced to 43.3% in the triplex tube without fins. Experiments were conducted to validate the proposed model. Simulated results correspond with the experimental results.

1. Introduction

Over the last three decades, the thermal energy storage of phase-change materials (PCMs) have been intensively studied by numerous researchers because of their high thermal energy densities per unit volume/mass and their potential for application in different engineering fields with wide temperatures ranges. PCM thermal energy storage is critical for eliminating the discrepancy between energy supply and demand as well as for improving the efficiency of solar energy systems. Thermal energy storage systems, especially latent heat thermal energy storage (LHTES), have recently gained considerable attention from the perspectives of global environmental problems and energy-efficiency improvement. LHTES demonstrates high performance and dependability with advantages of high storage capacity and nearly constant thermal energy [1]. PCM applications are found in different engineering fields such as thermal storage of building structures [2,3], building equipment such as domestic hot water, heating, and cooling systems [4–6], electronic products [7–9], drying technology [10], waste heat recovery [11], refrigeration and cold storage [12,13], solar air collectors [14], and solar cookers [15].

PCMs have limited use as thermal energy storage devices because of their low thermal conductivity. This disadvantage lengthens the time necessary to complete the melting and solidification processes. Several researchers investigated heat transfer enhancement in PCMs using various techniques such as the use of finned tubes [16], insertion of a metal matrix in the PCM [17], multitubes [18], bubble agitation in PCMs [19], PCM dispersed with high-conductivity particles [20], and multiple families of PCMs in LHTES [21]. Various fin configurations are applied to PCMs, including external and internal fins (circular, longitude, and rectangular). Erek et al. [16] investigated the behavior of thermal energy storage (shell and tube type) with a circular-finned tube and PCM in annular space. They developed a two-dimensional numerical model to predict the effect of fin dimensions and operation parameters (fin space, fin diameter, Re number, and heat transfer fluid inlet temperature) on the solidification and melting processes of PCM. Balikowski and Mollendorf [22] studied the effect of using a spined pipe tube and smooth pipe heat exchanger with two types of PCMs on the charging/discharging of a vertical double pipe heat exchanger with different PCMs in the annular gap. To improve the heat transfer of PCM thermal energy storage, Agyenim et al. [23] used circular and longitudinal fins to enhance heat transfer. They found that the longitudinal-finned system is suitable for charging and discharging in a concentric tube PCM system because such system can achieve optimal charge performance with negligible subcooling during discharge.

* Corresponding author at: Solar Energy Research Institute, University Kebangsaan Malaysia, Bangi, Selangor, Malaysia. Tel.: +60 389214596; fax: +60 389214593.
E-mail addresses: drsohif@gmail.com (S. Mat), abo_anas4@yahoo.com (A.A. Al-Abidi).

0196-8904/$ - see front matter © 2013 Elsevier Ltd. All rights reserved.
http://dx.doi.org/10.1016/j.enconman.2013.05.003

Nomenclature

C	mushy zone constant (kg/m^3 s)
Cp	specific heat of PCM (J/kg °C)
gi	gravity acceleration in the i-direction (m/s^2)
h	sensible enthalpy (J/kg)
H	enthalpy (J/kg)
k	thermal conductivity (W/m K)
L	latent heat fusion (J/kg)
P	pressure (Pa)
T	temperature (°C or K)
ui	velocity component (m/s)
r	tube radius (m)
Si	momentum source term in the i-direction (Pa/m)
Ste	Stefan number

Greek letters

ρ	fluid density (kg/m^3)
γ	liquid fraction
β	thermal expansion coefficient
μ	dynamic viscosity (kg/m s)
ε	constant

Subscripts

i, j	components
ini	initial
HTF	heat transfer fluid
m	melting
ref	reference
s	solidus of the PCM
l	liquidus of the PCM
t	time

Stritih [24] added a rectangular external fin to enhance heat transfer during melting and solidification of a latent heat storage for thermal applications in buildings. They found that heat storage (melting) was not a problem during thermal storage applications and that heat extraction (solidification) is effectively enhanced by fins. Blen et al. [25] investigated the melting and solidification characteristics of ($CaCl_2{\cdot}6H_2O$) as a PCM in a vertical two-concentric pipe energy storage system. Different design and operation

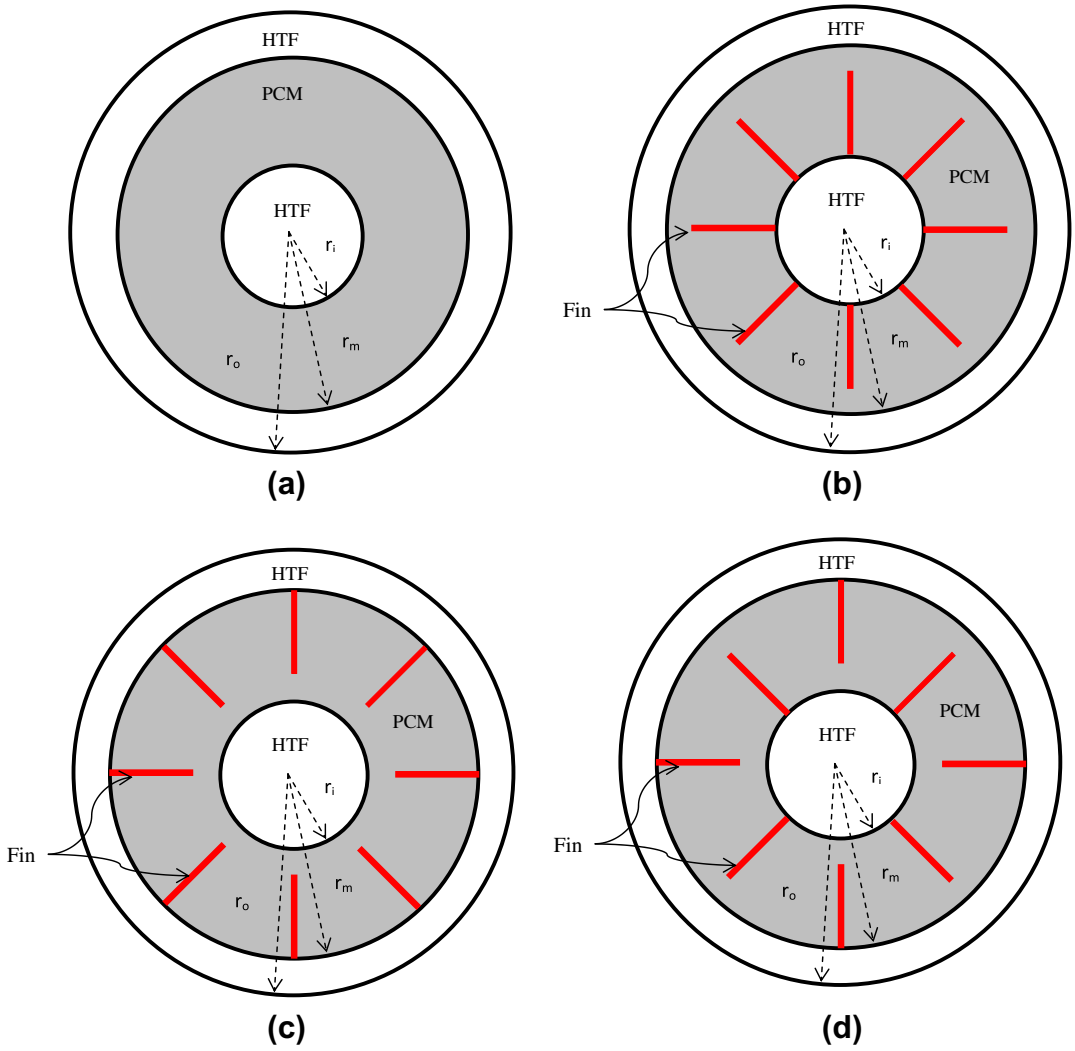

Fig. 1. The physical configuration of the TTHX models, (a) TTHX without fin, (b) TTHX with internal fins, (c) TTHX with external fin, (d) TTHX with internal–external fins.

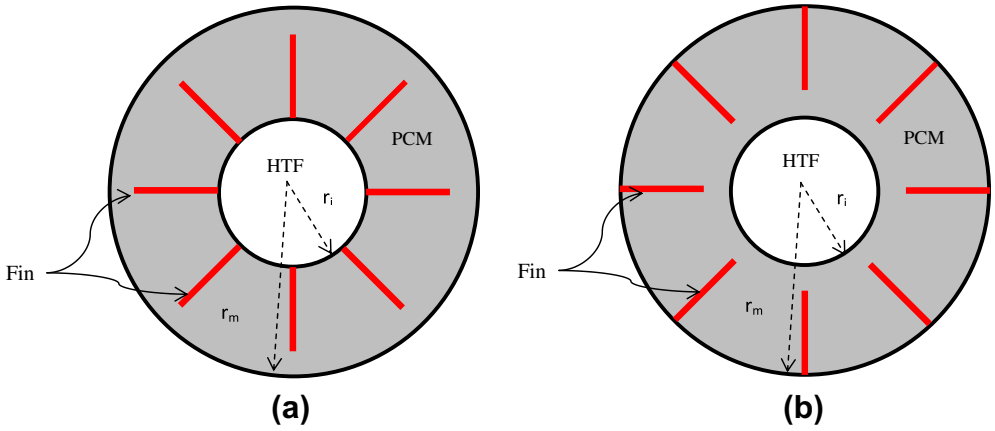

Fig. 2. Physical configurations (a) finned tube and (b) internally finned tube.

parameters were studied, including the number of fins inside the PCM, mass flow rate, and inlet heat transfer fluid (HTF) temperature. They found that the effect of design parameters is more significant than the effect of operation parameters. To reduce the charging and discharging time, Languri et al. [26] studied the effects of using a new thermal energy storage with high surface-to-volume and aspect ratios. They used a vertically sealed copper panel jointed axially with respect to the thermal energy storage center. Results showed that charging and discharging rates improved by nine times compared with the concentric system.

The time required to complete the melting and solidification of PCM is important to enable the absorption/release of solar thermal energy. The charging process depends on the HTF mass flow rate and inlet temperature. Inlet HTF temperature fluctuations affect the charging process, especially when the charging source depends on solar energy. To determine the time required for complete solidification, Ismail and Moraes [27] numerically and experimentally studied the effect of PCM container materials, configuration, and dimensions on the solidification of various PCMs. To meet the requirement to charge as quickly as possible, Agyenim et al. [28] increased the inlet HTF temperature between 125 and 145 °C when charging a double-pipe heat exchanger with PCM in the annulus side because daily solar availability in Europe for most of seasons is less than 8 h. They reported that overheating at the upper section and unequal heat distribution in the PCM occurs when the inlet HTF temperature exceeds 140 °C.

Al-Abidi et al. [29] introduced external and internal fins to the triplex-tube heat exchanger (TTHX) as a heat transfer-enhancement technique. They numerically investigated the effect of different design and operation parameters such as fin length, fin thickness, number of fins, and PCM geometries as well as TTHX materials on the melting process. The result showed that the melting time for the eight-cell PCM unit geometry was reduced to 34.7% compared with that of a triplex tube without fins.

TTHXs are used for different products and are utilized in the dairy, food, beverage, and pharmaceutical industries [30]. Long and Zhu [31] experimentally investigated triplex concentric tubes with PCM in the middle tube for the energy recovery of waste heat from air conditioning or solar energy, hot heat transfer fluid flowing in the outer tube during the charging process, and cold heat transfer fluid flowing in the inner tube during the releasing process. Khillarkar et al. [32] found that free convection significantly affected the melting of pure PCM contained in concentric horizontal annuli with different configurations: a square external tube with a circular tube inside and a circular external tube with a square tube inside.

TTHX with PCM in the middle tubes increases the heat-transfer area, consequently improving heat transfer relative to that of a double-pipe heat exchanger. The time required to complete PCM melting is also reduced. To charge the storage, a low temperature difference between the HTF inlet temperature and melting point of the PCM is used.

This numerical study compares the heat transfer during PCM melting in a triplex-tube heat exchanger based on three charging cases/approaches to complete PCM melting in 4 h. In the inside heating method, heat is supplied from the inner tube, and the outer tube is considered insulated. In the outside heating method, heat is delivered from the outer tube, and the inner tube is considered insulated. In the heating both sides method, heat is provided from the inner and outer tubes. During the melting process in the thermal storage, the effects of the longitudinal internal fin, external fin, and internal–external fins welded to the TTHX are investigated.

2. Numerical approach

2.1. Physical model

The physical configuration of the TTHX model is shown in Fig. 1. The model has a 25.4 mm inner tube radius (r_i) and 1.2 mm thickness. The middle tube (r_m) and outer tube radii (r_o) were 75 and 100 mm, respectively, with 2 mm thickness. Copper pipes were used to ensure high thermal conductivity. As shown in Fig. 1, eight fins 42 mm long and 1 mm thick were welded to the inner tube, middle tubes, and both tubes to enhance heat transfer. The same fin and tube dimensions were used for the finned and internally finned tubes, as shown in Fig. 2. The outer and inner tubes were used for HTF (water), whereas the middle tube was used for the PCM based on a commercially available material (Rubitherm GmbH-Germany (RT82)). The thermophysical properties are listed in Table 1.

Table 1
Thermo-physical properties of the PCM[a], copper.

Property	RT82	Copper
Density of PCM, solid, ρ_s (kg/m^3)	950	8978
Density of PCM, liquid, ρ_l (kg/m^3)	770	-
Specific heat of PCM, liquid, Cp_l, Cp_s (J/kg K)	2000	381
Latent heat of fusion, L (J/kg)	176000	-
Melting temperature, T_m (K)	350.15- 358.15	-
Thermal conductivity, k (W/m.K)	0.2	387.6
Thermal expansion coefficient (1/K)	0.001	-
Dynamic Viscosity, μ (kg/m.s)	0.03499	-

[a] Rubitherm GmbH, 2011. Available from: http://www.rubitherm.de.

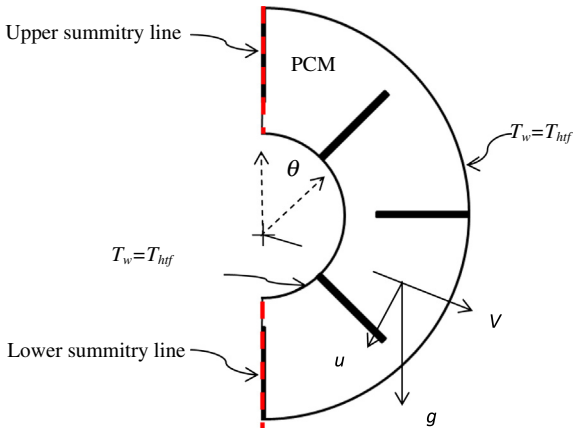

Fig. 3. Computational domain for all models of TTHX.

Table 2
Liquid fraction for different grid sizes with 0.5 s time step.

Grid size	Time (s)		
	300	1800	2700
17,956	0.1303	0.7013	0.9767
22,004	0.1283	0.6754	0.9738
27,854	0.1233	0.6529	0.9604

Table 3
Liquid fraction for different time steps with 17,956 grid size.

Time step (s)	Time (s)		
	300	1800	2700
0.2	0.1288	0.7204	0.9875
0.5	0.1303	0.7013	0.9767
1.0	0.1320	0.6885	0.9706

2.2. Governing equation

As regards the PCM inside the middle tube of the TTHX, mathematical equations of the melting process show a laminar, unsteady, and incompressible flow. Viscous dissipation is negligible. Constant thermophysical characteristics of the PCM such as the specific heat, thermal conductivity, and viscosity are considered in the analysis. The effect of natural convection during melting is considered by invoking the Boussinesq approximation, which is valid for the density variations of buoyancy force; otherwise, the effect is neglected. Density variation is defined as follows:

$$\rho = \rho_l/(\beta(T - T_l) + 1) \tag{1}$$

where ρ_l is the density of PCM at the melting temperature at T_l, and β is the thermal expansion coefficient. Viscous incompressible flow and temperature distribution are solved using the Navier–Stokes and thermal energy equations, respectively. The continuity, momentum, and thermal energy equations are respectively defined as follows [33]:

Continuity:

$$\partial_t(\rho) + \partial_i(\rho u_i) = 0 \tag{2}$$

Momentum:

$$\partial_t(\rho u_i) + \partial_j(\rho u_i u_j) = \mu\partial_{jj}u_i - \partial_i p + \rho g_i + S_i \tag{3}$$

The energy equation:

$$\partial_t(\rho h) + \partial_t(\rho\Delta H) + \partial_i(\rho u_i h) = \partial_i(k\partial_i T) \tag{4}$$

where ρ is the density of PCM (RT82), u_i is the fluid velocity, μ is the dynamic viscosity, p is the pressure, g is the gravity acceleration, k is the thermal conductivity, and h is the sensible enthalpy.

Sensible enthalpy can be expressed as follows:

$$h = h_{ref} + \int_{T_{ref}}^{T} Cp\Delta T \tag{5}$$

Enthalpy H can be defined as follows:

$$H = h + \Delta H \tag{6}$$

where h_{ref} is the reference enthalpy at the reference temperature T_{ref}, and Cp is the specific heat. ΔH is the latent heat content that changes between zero (solid) and L (liquid), which is the latent heat

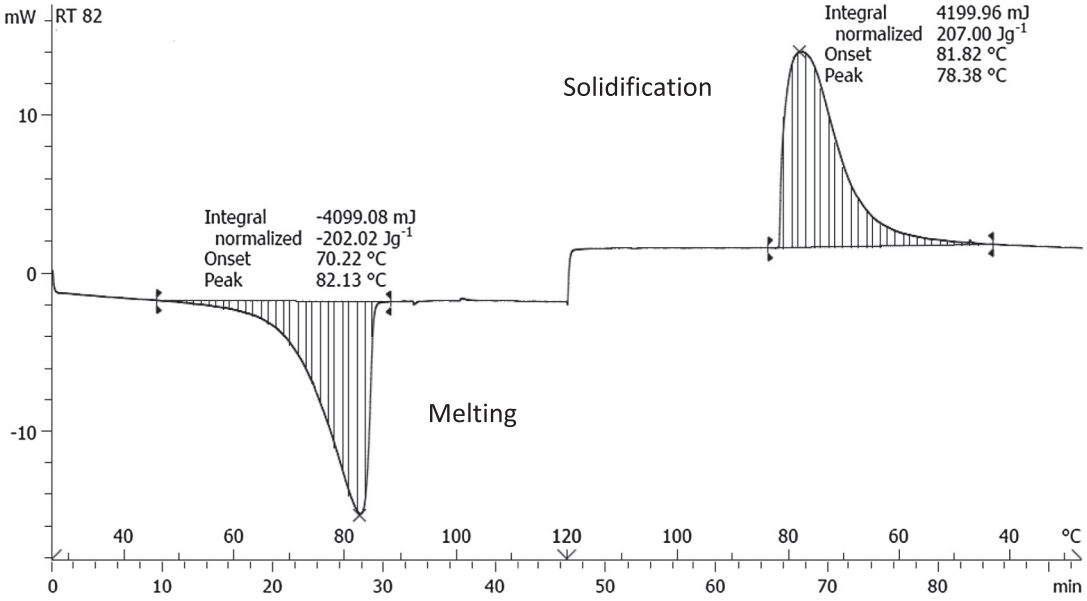

Fig. 4. DSC curves RT 82 PCM cooling and heating rate: 2 °C/min.

Table 4
Reported of mean and standard uncertainty of the PCM thermal properties.

Melting process			Solidification process		
Onset point (°C)	Peak point (°C)	Heat of fusion (KJ/kg)	Onset point (°C)	Peak Point (°C)	Heat of fusion (KJ/kg)
70.1275 ± 0.148172	82.17625 ± 0.047953	201.64375 ± 1.386656	81.86 ± 0.02828	78.158 ± 0.090358	207.807 ± 1.359165

of the PCM. γ is the liquid fraction that is generated during the phase change between the solid and liquid state when the temperature is $T_l \succ T \succ T_s$, which can be written as:

$$\gamma = \Delta H / L \tag{7}$$

$$\gamma = \begin{cases} 0 & \text{if } T \prec T_s \\ 1 & \text{if } T \succ T_l \\ \frac{(T-T_s)}{(T_l-T_s)} & \text{if } T_l \succ T \succ T_s \end{cases} \tag{8}$$

The source term S_i in momentum equation, Eq. (3), is defined as:

$$S_i = C(1-\gamma)^2 \frac{u_i}{\gamma^3 + \varepsilon} \tag{9}$$

where $C(1-\gamma)^2 \frac{u_i}{\gamma^3+\varepsilon}$ is the "porosity function" defined by Brent et al. [34] that enables the momentum equations to "mimic" Carmane Kozeny equations for flow in porous media. C is the constant reflection of the mushy zone morphology. C describes how steeply the velocity is reduced to zero when the material solidifies. This constant varies between 10^4 and 10^7 (10^5 is considered for this paper) [35]. ε is a small number (0.001) to prevent division by zero.

2.3. Initial and boundary conditions

At the initial time, PCM was solid, and temperature was 27 °C. A constant temperature of the tube wall represented the HTF temperature [36,37] which was at approximately 90 °C. The boundary conditions of the TTHX, finned tube, and internally finned tube were varied and can be written as follows:

Inside heating method and finned tube:

$$\text{at } r = r_i \rightarrow T = T_{\text{HTF}} \tag{10}$$

$$\text{at } r = r_m \rightarrow \frac{\partial T}{\partial r} = 0 \tag{11}$$

Outside heating method and internally finned tube:

$$\text{at } r = r_i \rightarrow \frac{\partial T}{\partial r} = 0 \tag{12}$$

$$\text{at } r = r_m \rightarrow T = T_{\text{HTF}} \tag{13}$$

Heating both sides method:

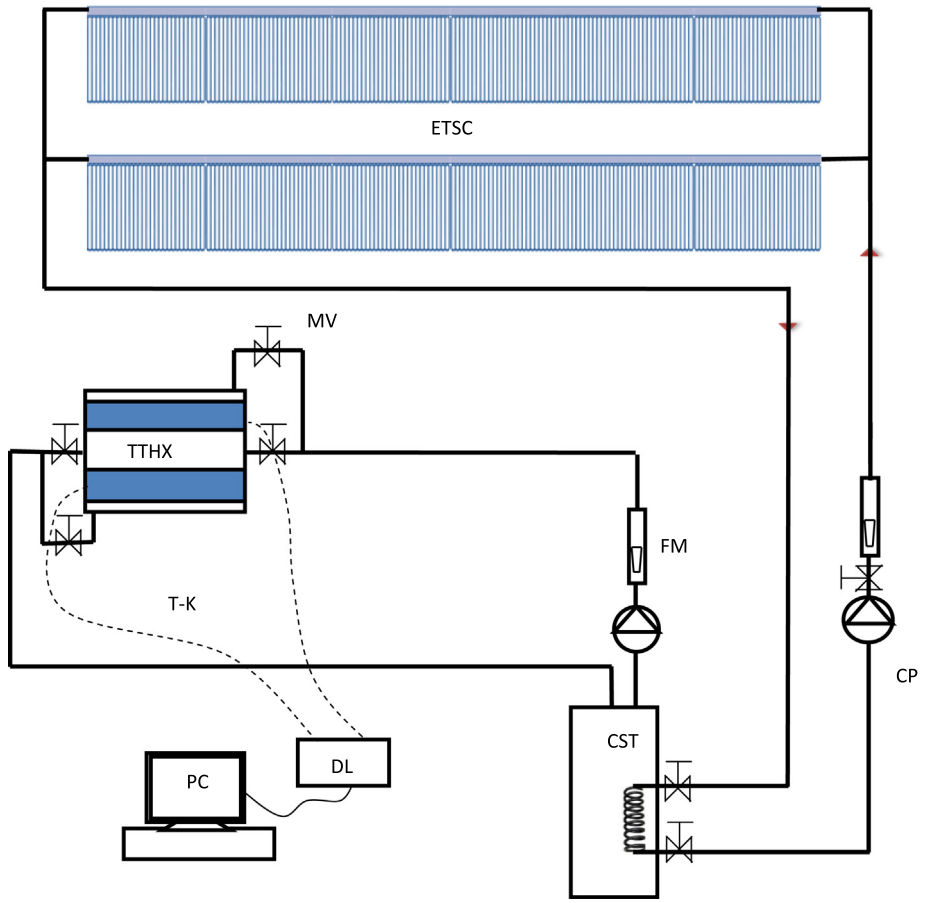

Fig. 5. Schematic diagram of the experimental apparatus which includes a triplex concentric tube's heat exchanger (TTHX), hot-water circulation pumps (CP), evacuated tube solar collector (ETSC), charging storage tank with electric heater (CST), rotameter to measure the flow rate (FM), manual shut off valve (MV), Data logger (DL), thermocouples type K (T-K), and personal computer (PC).

at $r = r_i \rightarrow T = T_{HTF}$ (14)

at $r = r_m \rightarrow T = T_{HTF}$ (15)

Initial temperature for all models:

at $t = 0 \rightarrow T = T_{ini}$ (16)

2.4. Numerical modeling

Modeling was conducted using FLUENT software based on the enthalpy–porosity technique and the finite volume method as described by Patankar [38]. In the enthalpy–porosity technique, the melt interface is not tracked explicitly. The liquid fraction indicates the fraction of the cell volume in liquid form and is a quantity associated with each cell in the domain. This parameter is computed at each iteration based on enthalpy balance. The mushy zone is a region where the liquid fraction lies between 0 and 1. This zone is modeled as a "pseudo" porous medium where porosity decreases from 1 to 0 as the material solidifies. When the material has fully solidified in a cell, porosity becomes zero, thus resulting in the drop of the velocity to zero. Details on the computational fluid dynamics application in the latent heat thermal energy storage can be found in Ref. [39].

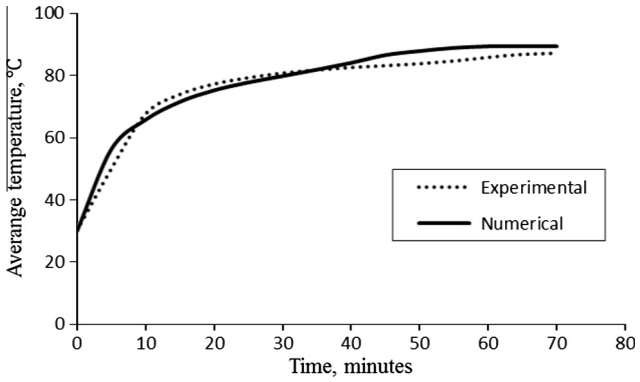

Fig. 7. Comparison of the experimental and numerical average temperature.

Fluent 6.3.26, a commercially available computer program, was used to establish the solidification and melting model for simulating the melting process of the PCM. Two dimensions (r and θ) of the TTHX are drawn and meshed in a geometric model. The mesh-generation software Gambit, which is part of the Fluent software package, helped define the boundary layers and zone types. The mesh

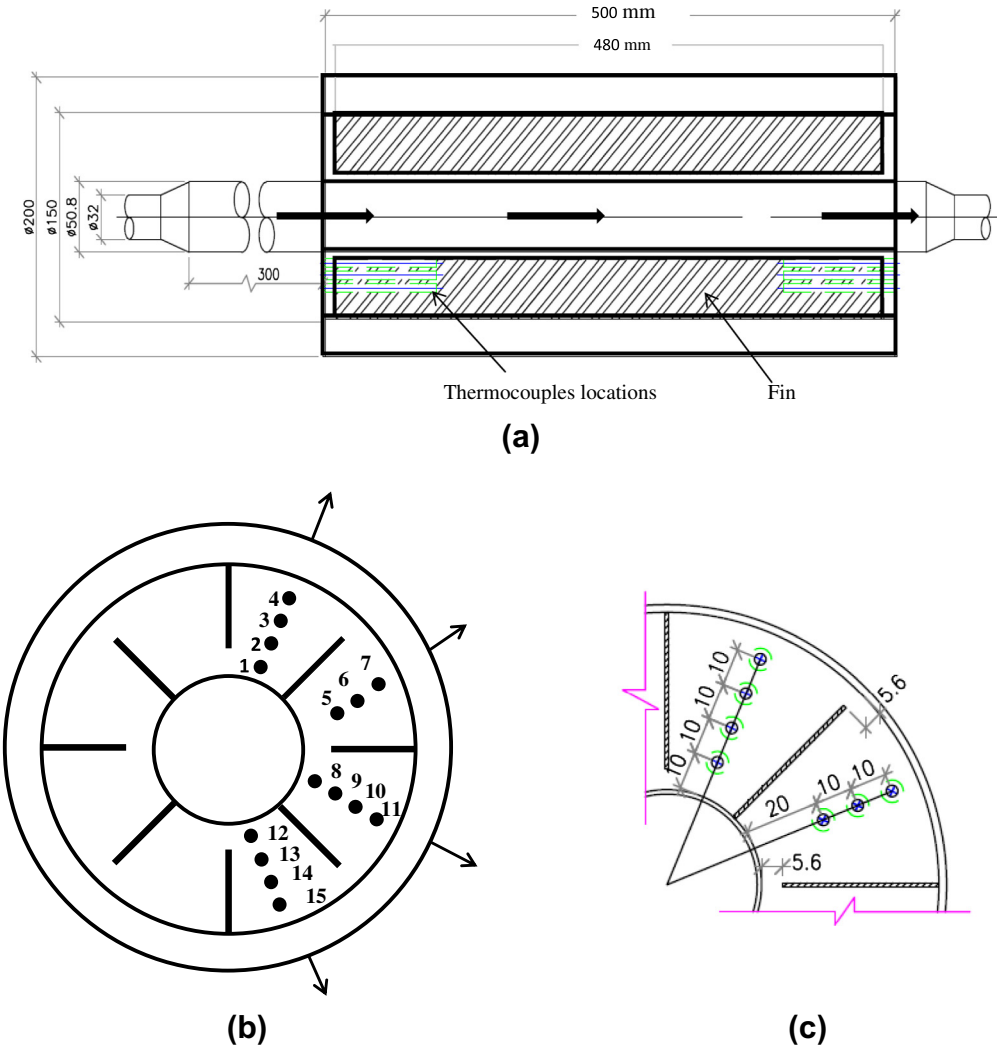

Fig. 6. Schematic diagram of the TTHX; (a) cross section of TTHX, (b) thermocouples distributions in TTHX, and (c) radial interval in the radial direction.

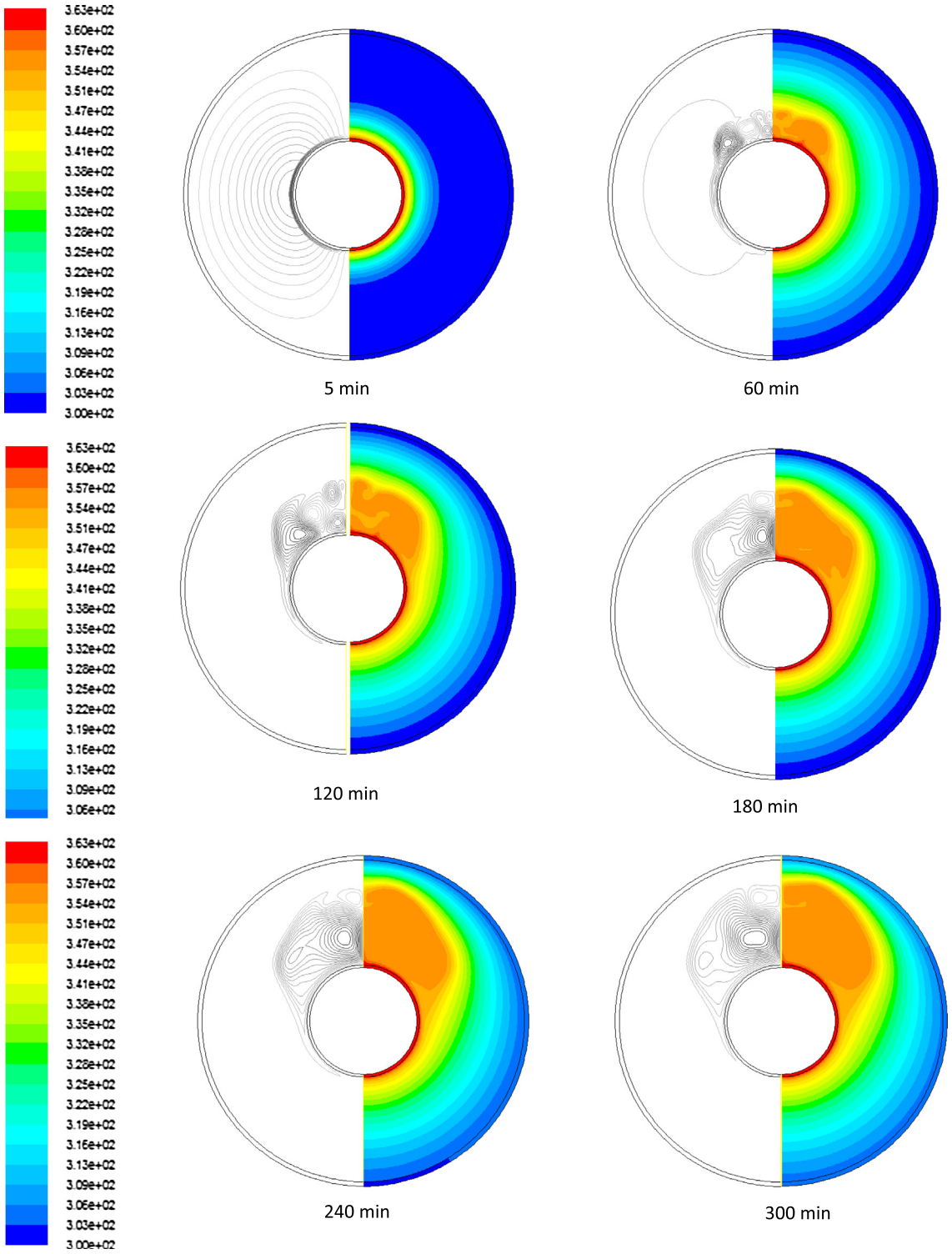

Fig. 8. Streamline, isothermal contour for the inside heating method.

was then exported to Fluent. A half-section computational grid is used to reduce the time required for simulation, as shown in Fig. 3. Fluent software uses the finite volume method described in [38], and employs the enthalpy–porosity formulation to solve the mass, velocity, and energy equations.

The PRESTO scheme is used for the pressure correction equation and the Semi-Implicit Pressure-Linked Equation algorithm was used for pressure–velocity coupling. The under relaxation value factors for pressure, velocity, energy, and liquid fraction are 0.3, 0.2, 1, and 0.9, respectively. The independence of the time steps from the melt fraction was examined for the simulations at 1, 0.5 (selected), and 0.2 s. Three grid sizes at 17,956 (chosen), 22,004, and 27,854 cells were investigated to validate the independence of grid size from the numerical solution. Tables 2 and 3 present

the liquid fractions for the three grid sizes and the time steps tested for the numerical model. The liquid fraction relates to the early, intermediate, and final stages of melting. A total of 17,956 cells with a 0.5 s time step was used for our calculation to achieve the predetermined convergence of the energy equation (10^{-5}) at 10^{-3} for the velocities.

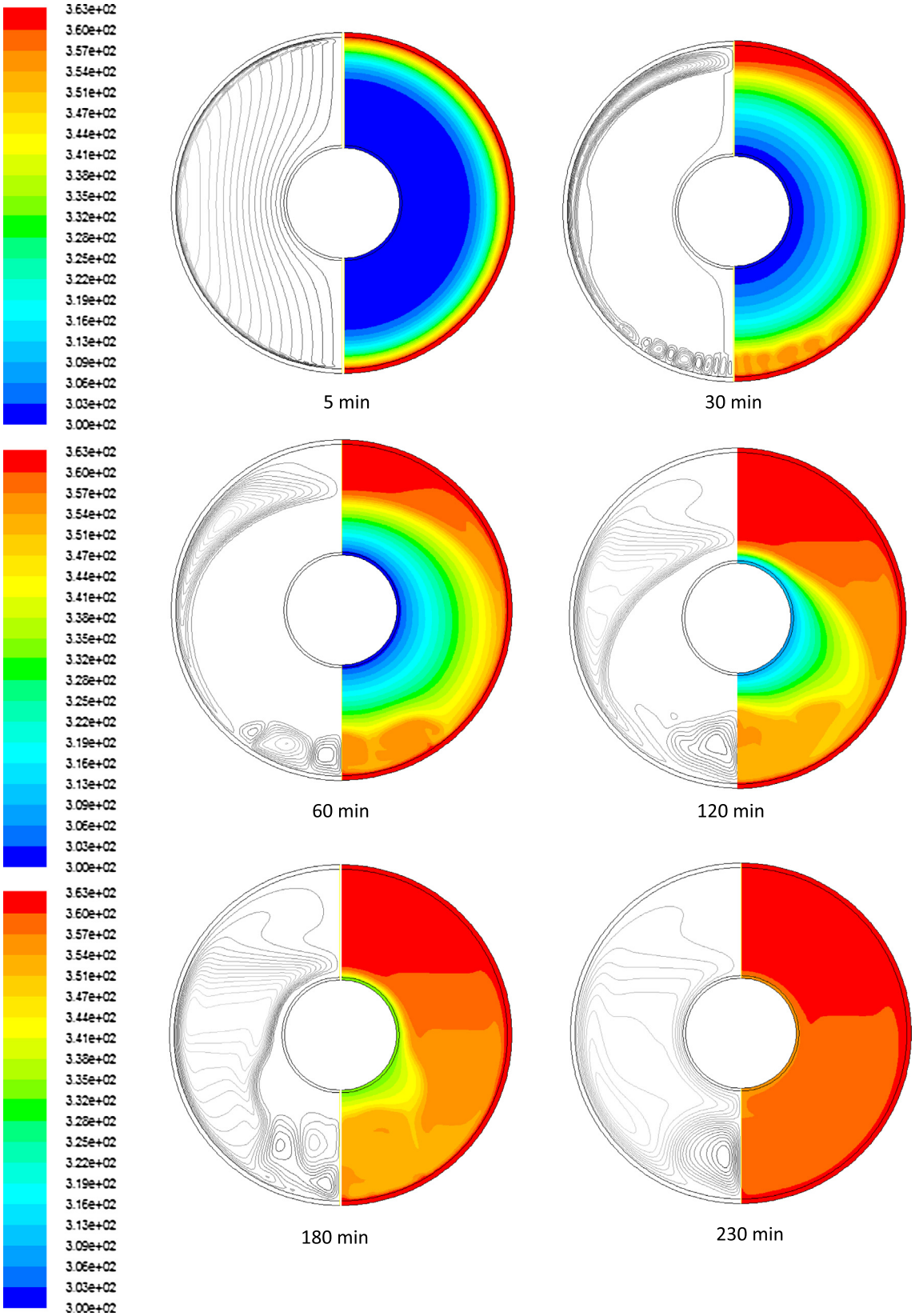

Fig. 9. Streamline, isothermal contour for the outside heating method.

3. Physical properties of the PCM and experimental apparatus and procedure

3.1. Phase change materials

To test the thermal properties of RT82 (heat of fusion, melting temperature, and solidification temperature), 20.29 mg of RT82 was used. Ten thermal cycling tests were repeated for the same sample. The material was heated from 27 °C ambient temperature to a maximum temperature of 120 °C at a heating rate of 2 °C/min. The cooling process was performed by cooling the PCM from 120 °C to ambient temperature at a cooling rate of 2 °C/min. The latent heat of fusion and melting temperature were measured using differential scanning calorimetry (METTLER TOLEDO; Model DSC1). Fig. 4 shows the relationship between temperature and heat flux of the sample for the melting and solidification of the PCM. Table 4 shows the average results and standard uncertainty of the melting and freezing temperatures of the material as well as the latent heat of fusion during the melting and freezing processes.

3.2. Experimental apparatus and procedure

A triplex concentric tube latent heat thermal storage was fabricated to validate the numerical model of the PCM melting process. Fig. 5 shows a schematic diagram of the experimental apparatus, which includes TTHX, hot-water circulation pumps, evacuated tube solar collector (ETSC), charging storage tank (CST) with electric heater, rotameter for measuring flow rate, and manual shut-off valve. Fig. 6 shows the TTHX section comprising three horizontally mounted concentric tubes with lengths of 500 mm and four longitudinal fins (42 mm fin pitch, 480 mm length, and 1 mm thick) welded onto each of the inner and middle tubes. The physical geometric parameters of the TTHX are given in the physical model section. Inner tube was extended to approximately 300 mm from the entrance to ensure that the flow will be fully developed. The data monitoring system comprised K-type thermocouples (measured at 0.5% accuracy), a data logger, and a personal computer to measure the temperatures in the PCM thermal storage. HTF flow rate was measured using a rotameter (measured at 5% accuracy). A total of 15 thermocouples were found fitted in the radial direction and at different angular directions in the PCM at 10 mm intervals. As shown in Fig. 6, the thermocouples were located 100 mm from the entrance of the HTF tube in the thermal storage. A 70 mm thick glass wool insulation was wrapped around the TTHX to decrease heat loss and insulate the surface.

As shown in Fig. 5, the hot water used in the charging process was delivered from a central heating station in the Green Technology Park at the Solar Research Energy Institute, National University

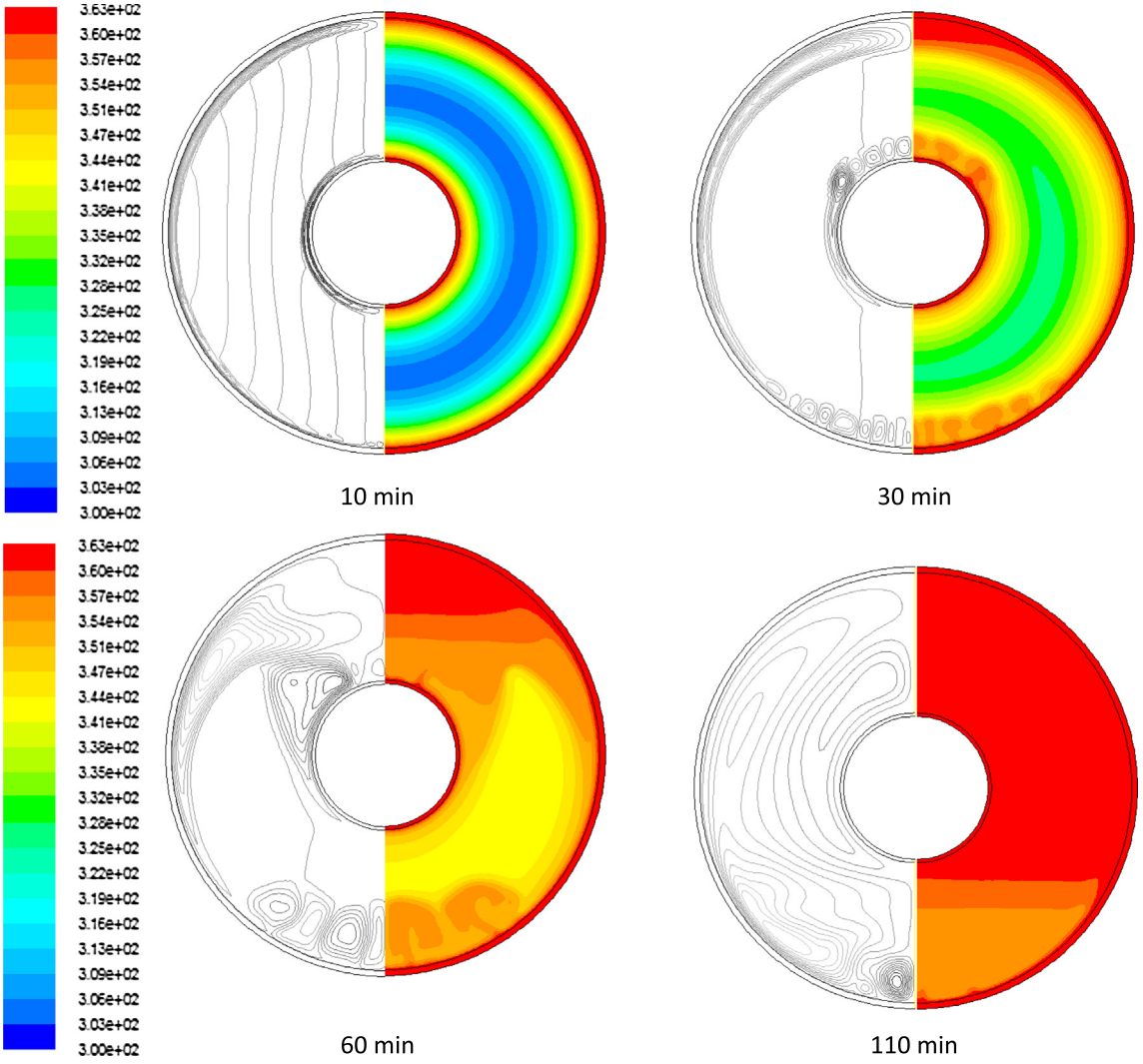

Fig. 10. Streamline, isothermal contour for the heating both sides method.

of Malaysia. This heating station was designed to deliver the hot water required by various solar-thermal systems. The central heating station consists of 300 evacuated tube solar collectors with three 200 L storage tanks. One storage tank was used for the current application. The TTHX was filled with 5.6 kg PCM, and no leakage was observed. Charging started when the CST reached 90 °C.

3.3. Validation of the numerical model

To validate the numerical model, the melting model created using Fluent 6.3.26 was compared with an experimental model. The average temperature of the PCM was 27 °C when melting started, whereas HTF temperature was 90 °C. HTF temperature was maintained in the CST using an electrical heater and a thermostat controller. The mass flow rate of the HTF was 8.3 l/min. The latent heat of fusion was 176,000 J/kg whereas the melting range of the PCM was between 70 °C and 82 °C, depended on the experimental test. Fig. 7 shows the comparison of the average temperature vs. time of PCM, which was determined using the 15 thermocouples inserted in the PCM at the HTF tube entrance, with that of the numerical model. The results of the present model corresponded with the experimental results.

4. Results and discussion

4.1. Heating methods

Three heating methods were used to charge the TTHX without fins. The inside heating approach is the most commonly used method in TTHX applications, such as in [40]. Outside heating methods were used in [31]. The heating of both sides method is typically used in food processing, where TTHX is often employed. The heating of both sides method is investigated in this study to highlight the predicted enhancement of LHTES performance.

4.1.1. Inside heating method

Fig. 8 shows the contours of the streamlines, the left half of each circle, and the colorized isotherm, the right half of each circle in the inside heating method for different time periods (5, 60, 120, 180, 240, and 300 min). Heat transfer occurred between the hot wall of the tube and the solid surface of the PCM by conduction which dominated the melting process at the early stage and caused a thin layer of liquid to form in the narrow melting area because of heat transfer. Several convection cells were formed and subsequently expanded to the upper part of the tube. The liquid fraction increased in the upper part of the tube, whereas the rest of the PCM remained solid without any phase change at the bottom of the tube. Over time, cell convection emerged and facilitated the formation of two large convection cells at 240 min. As shown in Fig. 10, the hotter liquid of PCM was pushed upward to the top of the tubes because of natural convection effects driven by buoyancy. On the other hand, the solid part of the PCM was squeezed down to the bottom of the tube because of heavier density. After 300 min of heating, the PCM did not melt, which indicates that this method was slow and required more time than that predetermined by our application.

4.1.2. Outside heating method

Fig. 9 shows the contours of the streamlines (left) and colorized isotherm (right) of each circle of the outside heating method for different time periods (5, 30, 60, 120, 180, and 230 min). Numerous circulations formed at the bottom region of the annulus because of the small melting area after 30 min. On the other hand, a large convection cell formed in the upper part of the annulus. By the time advancing the convection cells were combined in the bottom region to create a three cells and the convection cell was expanded in the upper part of the annulus (60 min), the bottom cells were emerged with the upper cell after 120 min. Complete melting was achieved after 230 min, which was considered an improvement over the inside heating method. This result is attributed to the increase in the heat transfer surface, which became three times larger than that in the inside heating method.

4.1.3. Heating both sides method

Fig. 10 illustrates the colorized isotherm line in the right-half section and the streamline in the left-half section of the symmetry circle. Several small convection cells were created on the upper region of the inside tube and at the bottom section of the outside

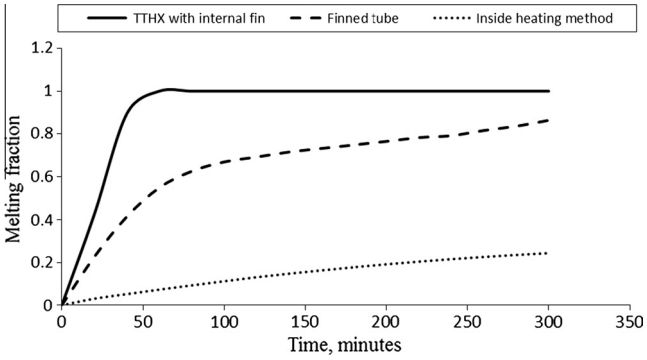

Fig. 11. Melting fraction vs. time for the inside heating method, finned tube, and TTHX with Internal fin.

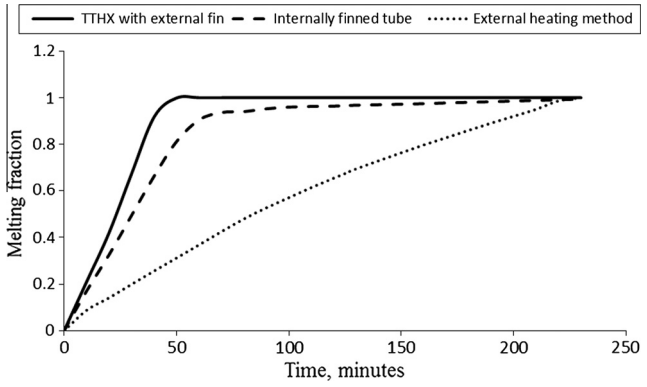

Fig. 12. Melting fraction vs. time for the outside heating methods, internally finned tube, and TTHX with external fin.

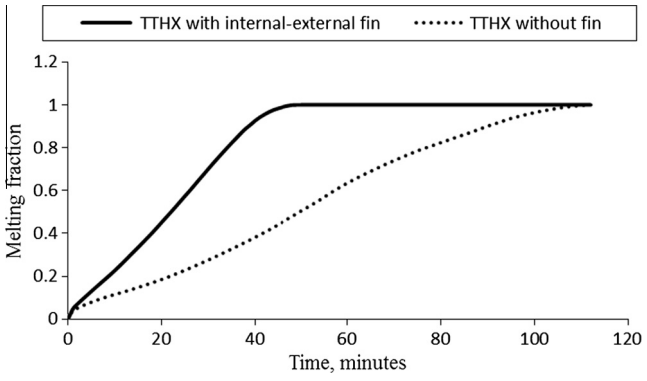

Fig. 13. Melting fraction vs. time for the TTHX with and without fins.

tube. After 30 min, liquid was formed on the long tube circumference of the outside tube, which generated a large convection cell on the outside tube. Over time circulation cells in the upper region of the inside tube emerged with the convection cell in the upper zone of the outside tube. This result is attributed to the natural convection created when liquid PCM was squeezed into this region after 60 min of melting. Three convection cells were formed in the upper part of the annulus. The convection cells in the annulus combined, and significant natural convection accelerated the melting process. A complete phase transition was observed after 110 min of melting.

4.2. Fin embedded heat transfer enhancement

The application of fins embedded in the PCM is the basis of most heat enhancement techniques because of its simplicity, easy fabrication, and low construction cost [1]. The effects of fins welded to the inside tube, middle tube, and both tubes on the PCM melting

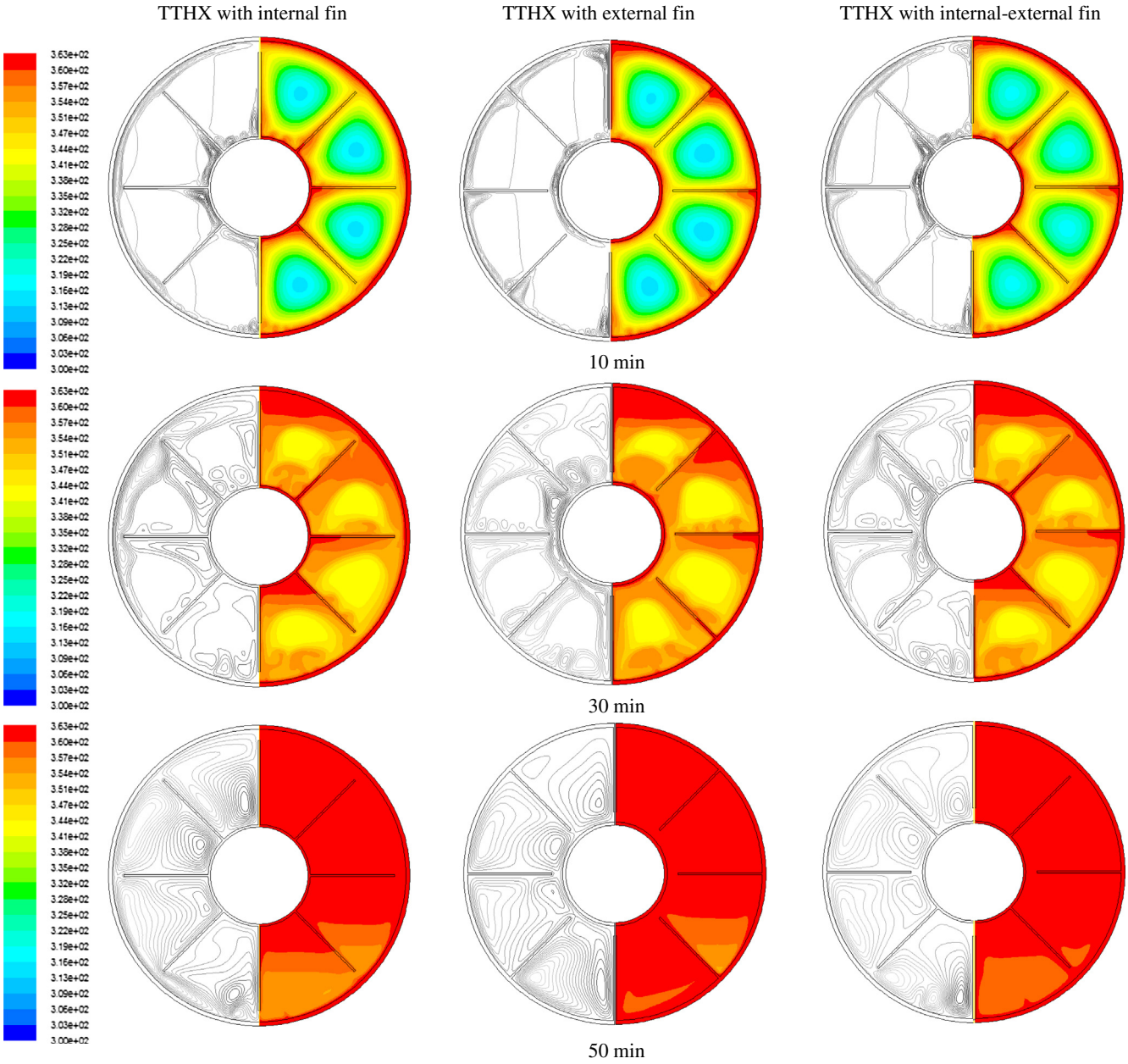

Fig. 14. Streamline, isothermal contour for the TTHX with internal fin, TTHX with external fin, TTHX with internal–external fin.

Table 5
The melting time percentage for different fin length of the three enhancements methods (%).

TTHX without fin	TTHX with internal fin Fin length (mm)				TTHX with external fin Fin length (mm)				TTHX with internal–external fin Fin length (mm)			
	10	20	30	42	10	20	30	42	10	20	30	42
100	81.2	66	55.3	48.2	70.5	53.5	47	46	73.9	60.8	47.8	43.4

process in the TTHX were investigated. Numerical results for the enhancement techniques using three heating methods of the TTHX without fin as well as with a normal finned tube and internally finned tube were compared.

4.2.1. Internal fin heat transfer enhancement

Fig. 11 shows the melting fraction vs. time of melting for the inside heating method, finned tube which is used by numerous researchers to enhance heat transfer for a double-pipe heat exchanger and for TTHX with an internal fin welded to the inner tube. The melting fraction of the normal tube was observed to be slow. After 300 min of melting, approximately 76% of the PCM was in the solid state. Better enhancement was achieved by using the finned tube. The melting process was accelerated after 90 min, after which it slowed down because of un-melted specimen in the annulus. Complete melting was difficult to achieve at the bottom region of the annulus because natural convection transferred most of the heat to the upper region. This behavior was also observed in [23]. Complete melting was achieved using TTHX with an internal fin welded to the inner tube. A significant effect was observed on the heat transfer between the PCM and hot-wall tube, because of which the whole PCM melted after 54 min.

4.2.2. External fin heat transfer enhancement

Fig. 12 illustrates the melting fraction vs. time of the external heating methods, internally finned tube, and TTHX with external fin. Complete melting was achieved after 230 min for the external heating methods. Melting rate was enhanced by using the internally finned tube. Approximately 90% of the PCM melted after 60 min. Un-melted PCM on the inside tube took a longer time to melt because convection circulation formed away from the bottom side of the inside tube, as shown in Fig. 9 (180 min). Melting rate significantly improved after using a TTHX with external fins welded to the middle tube. The whole PCM in the annulus changed to the liquid state after 52 min compared with the external heating and internally finned tube methods.

4.2.3. Internal–external fin heat transfer enhancement

Fig. 13 shows the melting fraction vs. time for the TTHX with and without fins. As predicted, complete melting for the PCM was achieved using the two methods, which consumed approximately 110 min for the TTHX without fins because of the additional heat transfer surfaces when using this method compared with the inside and outside methods. The melting process was enhanced by the addition of fins to the inner and middle tubes. The whole PCM melted after 49 min.

4.3. Comparison of melting process of the three enhancements techniques

Fig. 14 shows the streamline and temperature contours for the TTHX with internal fin, TTHX with external fin, and TTHX with internal fin-external fin. The flow field comprises multiple convection cells after 10 min of melting. Warm temperatures spread relatively quickly through the inner, middle, and fin walls. Over time, melting was affected by the natural convection established in the thermal storage. Flow increased after 30 min of melting under the three techniques. No differences among the three methods were found, except that the melting rate of the internal–external fin was faster for a 42 mm fin length, as shown in Table 5. This result is attributed to the effect of natural convection that hastened the melting process.

4.4. Fin length effect on the melting rate

Fig. 15a–d shows the effect of fin length on the melting process of the three enhancement methods. The fin lengths investigated were 10, 20, 30, and 42 mm. As shown in Fig. 15a–d, melting time decreased as fin length increased. Significant enhancement in the thermal performance of the storage was achieved by using the three methods at any stage of melting. TTHX with external fin achieved complete melting at a relatively earlier time for fin

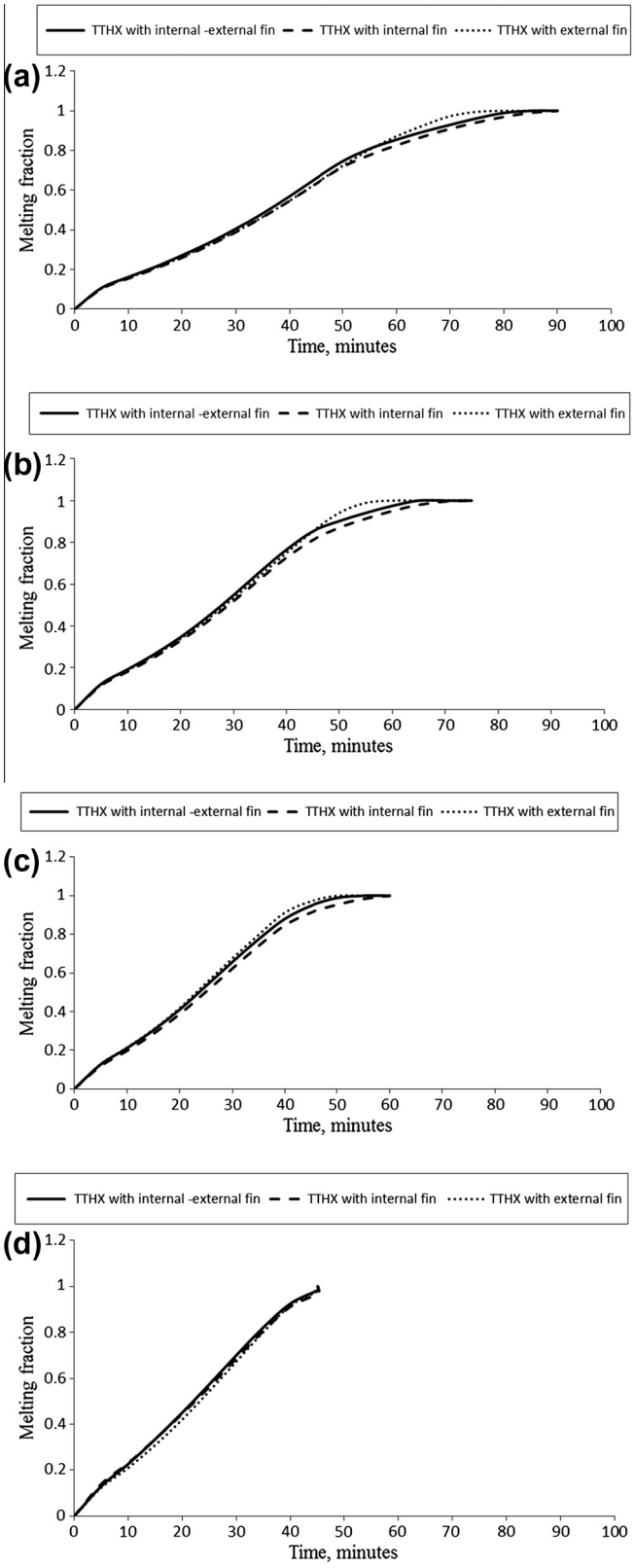

Fig. 15. Effect of the fin length for the three enhancement methods in TTHX, (a) 10 mm, (b) 20 mm, (c) 30 mm, (d) 42 mm.

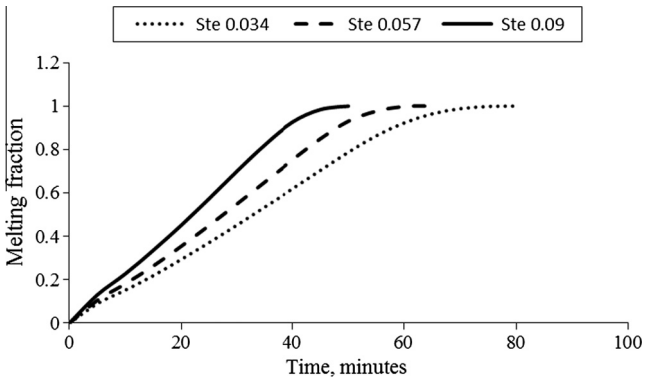

Fig. 16. Stefan number effect to the melting time.

lengths of 10, 20, and 30 mm followed by TTHX with internal–external fin method. To distinguish between these three enhancements methods, the percentages of melting time of the three methods with respect to the TTHX without fin are listed in Table 5. Table 5 shows that the energy charge rate is enhanced by 43.4% for a 42 mm fin length in the TTHX with internal–external fin method.

4.5. Stefan number effect on melting rate

Fig. 16 shows the melting fraction vs. time for three Stefan numbers: 0.034, 0.057, and 0.09 (temperature difference of 3, 5, and 8 °C, respectively), which described the melting process in the TTHX with internal–external fin. The Stefan number is defined as follows:

$$\mathrm{Ste} = \frac{Cp_l(T - T_m)}{L} \tag{17}$$

where Cp_l is the specific heat of the liquid PCM, L is the latent heat of PCM, and T_m is the melting temperature of PCM. The Stefan number shows the difference between the surface temperature and melting temperature of the PCM related to the latent heat of fusion. This difference affects the melting rate. As shown in Fig. 16, the Stefan number affects the melting rate in that a larger Stefan number causes a faster increase in the melting fraction and a lower melting time.

5. Conclusion

The melting process for RT 82 used as a PCM in a TTHX was studied numerically. Inside tube heating, outside tube heating, and heating of both sides methods for charging the PCM were investigated using the simulation program Fluent 6.3.26. Three heat transfer enhancement methods, namely, TTHX with internal fin, TTHX with external fin, and TTHX with internal–external fin, were studied to improve the thermal performance of PCM thermal storage. The results indicate no significant difference among the three enhancement techniques in terms of the PCM melting rate. Complete melting using internal–external fin with 42 mm fin length was reduced to 43.3% compared with that of TTHX without fin. The models were validated experimentally, and results were found to correspond with experimental studies.

References

[1] Al-Abidi AA, Bin Mat S, Sopian K, Sulaiman MY, Lim CH, Th A. Review of thermal energy storage for air conditioning systems. Renew Sustain Energy Rev 2012;16:5802–19.
[2] Caliskan H, Dincer I, Hepbasli A. Thermodynamic analyses and assessments of various thermal energy storage systems for buildings. Energy Convers Manage 2012;62:109–22.
[3] Joulin A, Younsi Z, Zalewski L, Lassue S, Rousse DR, Cavrot J-P. Experimental and numerical investigation of a phase change material: thermal-energy storage and release. Appl Energy 2011;88:2454–62.
[4] Zukowski M. Mathematical modeling and numerical simulation of a short term thermal energy storage system using phase change material for heating applications. Energy Convers Manage 2007;48:155–65.
[5] Hamada Y, Fukai J. Latent heat thermal energy storage tanks for space heating of buildings: comparison between calculations and experiments. Energy Convers Manage 2005;46:3221–35.
[6] Benli H. Energetic performance analysis of a ground-source heat pump system with latent heat storage for a greenhouse heating. Energy Convers Manage 2011;52:581–9.
[7] Shatikian V, Ziskind G, Letan R. Numerical investigation of a PCM-based heat sink with internal fins: constant heat flux. Int J Heat Mass Transfer 2008;51:1488–93.
[8] Wang Y-H, Yang Y-T. Three-dimensional transient cooling simulations of a portable electronic device using PCM (phase change materials) in multi-fin heat sink. Energy 2011;36:5214–24.
[9] Yang Y-T, Wang Y-H. Numerical simulation of three-dimensional transient cooling application on a portable electronic device using phase change material. Int J Therm Sci 2012;51:155–62.
[10] Çakmak G, Yıldız C. The drying kinetics of seeded grape in solar dryer with PCM-based solar integrated collector. Food Bioprod Process 2011;89:103–8.
[11] Pandiyarajan V, Chinna Pandian M, Malan E, Velraj R, Seeniraj RV. Experimental investigation on heat recovery from diesel engine exhaust using finned shell and tube heat exchanger and thermal storage system. Appl Energy 2011;88:77–87.
[12] Oró E, Miró L, Farid MM, Cabeza LF. Improving thermal performance of freezers using phase change materials. Int J Refrig 2012;35:984–91.
[13] He Q, Wang S, Tong M, Liu Y. Experimental study on thermophysical properties of nanofluids as phase-change material (PCM) in low temperature cool storage. Energy Convers Manage 2012;64:199–205.
[14] Mahmud A, Sopian K, Alghoul MA, Sohif M. Using a paraffin wax–aluminum compound as a thermal storage material in solar air heater. J Eng Appl Sci 2009;4:74–7.
[15] Sharma SD, Iwata T, Kitano H, Sagara K. Thermal performance of a solar cooker based on an evacuated tube solar collector with a PCM storage unit. Sol Energy 2005;78:416–26.
[16] Erek A, İlken Z, Acar MA. Experimental and numerical investigation of thermal energy storage with a finned tube. Int J Energy Res 2005;29:283–301.
[17] Cabeza LF, Mehling H, Hiebler S, Ziegler F. Heat transfer enhancement in water when used as PCM in thermal energy storage. Appl Therm Eng 2002;22:1141–51.
[18] Agyenim F, Eames P, Smyth M. Heat transfer enhancement in medium temperature thermal energy storage system using a multitube heat transfer array. Renew Energy 2010;35:198–207.
[19] Velraj R, Seeniraj RV, Hafner B, Faber C, Schwarzer K. Heat transfer enhancement in a latent heat storage system. Sol Energy 1999;65:171–80.
[20] Mettawee E-BS, Assassa GMR. Thermal conductivity enhancement in a latent heat storage system. Sol Energy 2007;81:839–45.
[21] Mosaffa AH, Infante Ferreira CA, Talati F, Rosen MA. Thermal performance of a multiple PCM thermal storage unit for free cooling. Energy Convers Manage 2013;67:1–7.
[22] Balikowski JR, Mollendorf JC. Performance of phase change materials in a horizontal annulus of a double-pipe heat exchanger in a water-circulating loop. J Heat Transfer 2007;129:265–72.
[23] Agyenim F, Eames P, Smyth M. A comparison of heat transfer enhancement in a medium temperature thermal energy storage heat exchanger using fins. Sol Energy 2009;83:1509–20.
[24] Stritih U. An experimental study of enhanced heat transfer in rectangular PCM storage. Int J Heat Mass Transfer 2004;47:2841–7.
[25] Blen K, Takgil F, Kaygusuz K. Thermal energy storage behavior of $CaCl_2{\cdot}6H_2O$ during melting and solidification. Energy Sources A Recov Util Environ Eff 2008;30:775–87.
[26] Languri EM, Aigbotsua CO, Alvarado JL. Latent thermal energy storage system using phase change material in corrugated enclosures. Appl Therm Eng 2013;50:1008–14.
[27] Ismail KAR, Moraes RIR. A numerical and experimental investigation of different containers and PCM options for cold storage modular units for domestic applications. Int J Heat Mass Tranfer 2009;52:4195–202.
[28] Agyenim F, Eames P, Smyth M. Experimental study on the melting and solidification behaviour of a medium temperature phase change storage material (Erythritol) system augmented with fins to power a $LiBr/H_2O$ absorption cooling system. Renew Energy 2011;36:108–17.
[29] Al-Abidi AA, Mat S, Sopian K, Sulaiman MY, Mohammad AT. Internal and external fin heat transfer enhancement technique for latent heat thermal energy storage in triplex tube heat exchangers. Appl Therm Eng 2013;53:147–56.
[30] García-Valladares O. Numerical simulation of triple concentric-tube heat exchangers. Int J Therm Sci 2004;43:979–91.
[31] Long J-Y, Zhu D-S. Numerical and experimental study on heat pump water heater with PCM for thermal storage. Energy Build 2008;40:666–72.

[32] Khillarkar DB, Gong ZX, Mujumdara AS. Melting of a phase change material in concentric horizontal annuli of arbitrary cross-section. Appl Therm Eng 2000;20:893–912.
[33] Darzi AR, Farhadi M, Sedighi K. Numerical study of melting inside concentric and eccentric horizontal annulus. Appl Math Model 2012;36:4080–6.
[34] Brent AD, Voller VR, Reid KJ. Enthalpy-porosity technique for melting convection-diffusion phase change: application to the melting of a pure metal. Numer Heat Transfer 1988;13:297–318.
[35] Ye W-B, Zhu D-S, Wang N. Numerical simulation on phase-change thermal storage/release in a plate-fin unit. Appl Therm Eng 2011;31:3871–84.
[36] Guo C, Zhang W. Numerical simulation and parametric study on new type of high temperature latent heat thermal energy storage system. Energy Convers Manage 2008;49:919–27.
[37] Hosseini M, Ranjbar A, Sedighi K, Rahimi M. A combined experimental and computational study on the melting behavior of a medium temperature phase change storage material inside shell and tube heat exchanger. Int Commun Heat Mass Transfer 2012;39:1416–24.
[38] Patankar SV. Numerical heat transfer and fluid flow. New York: McGraw Hill; 1980.
[39] Al-Abidi AA, Mat SB, Sopian K, Sulaiman MY, Mohammed AT. CFD applications for latent heat thermal energy storage: a review. Renew Sust Energy Rev 2013;20:353–63.
[40] Ismail KAR, Alves CLF. Phase change thermal energy storage in shell and circular-tube annulus configuration. In: Nejat T, Veziroglu B, editors. Alternative energy sources. Miami: Hemisphere Publishing Corporation; 1987.